Natural Resources Canada | Ressources naturelles Canada

GEOLOGICAL SURVEY OF CANADA
OPEN FILE 8968

Laser ablation inductively coupled plasma mass spectrometry mapping of porphyry-related epidote from south-central British Columbia

A. Plouffe, D.C. Petts, I.M. Kjarsgaard, and M. Polivchuk

2023

Canada

GEOLOGICAL SURVEY OF CANADA
OPEN FILE 8968

Laser ablation inductively coupled plasma mass spectrometry mapping of porphyry-related epidote from south-central British Columbia

A. Plouffe[1], D.C. Petts[1], I.M. Kjarsgaard[2], and M. Polivchuk[1]

[1]Geological Survey of Canada, 601 Booth Street, Ottawa, Ontario
[2]Mineralogical Consultant, 15 Scotia Place, Ottawa, Ontario

2023

Permanent link: https://doi.org/10.4095/331671

This publication is available for free download through GEOSCAN (https://geoscan.nrcan.gc.ca/).

Recommended citation
Plouffe, A., Petts, D.C., Kjarsgaard, I.M., and Polivchuk, M., 2023. Laser ablation inductively coupled plasma mass spectrometry mapping of porphyry-related epidote from south-central British Columbia; Geological Survey of Canada, Open File 8968, 1 .zip file. https://doi.org/10.4095/331671

Publications in this series have not been edited; they are released as submitted by the author.

ISSN 2816-7155
ISBN 978-0-660-48118-0
Catalogue No. M183-2/8968E-PDF

Contents

List of figures

13. A) BSE image of an epidote grain (grain 1) from till sample 12PMA095 at Mount Polley. B) to H) are examples of LA-ICP-MS maps (As, Sb, MgO, CaO, TiO_2, Y, P_2O_5). Chl – chlorite, Tnt – titanite Bt – biotite,
14. A) BSE image of an epidote grain (grain 2) from till sample 12PMA095 at Mount Polley. B) to G) are examples of LA-ICP-MS maps (As, Sb, K2O, TiO_2, Cu, La). Bt – biotite

List of appendices

1. Sample location information and brief notes about each sample.
2. LA-ICP-MS geochemical maps and analytical results.

Abstract

The microscopic composition of thirteen samples of epidote related to porphyry Cu mineralization was mapped using laser ablation inductively coupled plasma mass spectrometry (LA-ICP-MS) at the Geological Survey of Canada. The objective of this research is to improve the indicator mineral method of mineral exploration in glaciated terrains by utilizing the trace element composition of epidote. The analyzed samples include epidote from two bedrock samples at each of the following porphyry Cu deposits of south-central British Columbia: Gibraltar, Mount Polley and Woodjam. Epidote from three bedrock samples of Nicola Group which are proximal (<2 km) and distal (12 km) to known porphyry mineralization, and four epidote grains from two till samples, one at Gibraltar and a second one at Mount Polley, were also analyzed. Backscattered electron (BSE) images and the LA-ICP-MS maps show a heterogeneous distribution of Fe and Al in epidote following complex and mottled patterns. Trace elements are heterogeneously distributed in epidote following the Fe-Al zoning in some samples. Evidence of late infiltration of trace elements (e.g., Cu, Zn, and REE) along fractures in epidote is observed. Multiple LA-ICP-MS spot analyses need to be conducted on this mineral to fully evaluate its composition as an indicator mineral of porphyry Cu mineralization.

Introduction

This open file is a data depository of geochemical maps of epidote obtained by laser ablation inductively coupled plasma mass spectrometry (LA-ICP-MS) at the Geological Survey of Canada (GSC). Research on the geochemical composition of epidote was done as part of a Targeted Geoscience Initiative (TGI) project on hydrothermal ore systems. This research aims to improve mineral exploration methods in glaciated terrains by utilizing epidote as a geochemical indicator of porphyry Cu mineralized source rocks (Plouffe et al., 2021a, 2022). Tracing the source of indicator minerals, such as epidote, in till will improve our capacity of detecting mineralization buried by a glacial sediment cover. Mapping the composition of epidote by LA-ICP-MS provides information about the formation and evolution of porphyry Cu systems and serves to link the characteristics of this mineral to porphyry Cu deposits.

This open file presents thirteen LA-ICP-MS maps of epidote from:

1. Six bedrock samples including two samples from each of the following porphyry Cu deposits located in south-central British Columbia: Gibraltar, Mount Polley and Woodjam (Fig. 1);
2. Three bedrock samples of Nicola Group that is the main regional bedrock unit host of the porphyry intrusions: two samples close to an intrusion that hosts mineralization (<1 km; Gibraltar and Woodjam) and one approximately 12 km from Mount Polley; and,
3. Two epidote grains in each of two till samples: one from Gibraltar and a second one from Mount Polley, for a total of four grains.

The open file includes a short description of the element distribution within epidote and a discussion on the interpretation of the distribution patterns.

Background and geological setting

Epidote is abundantly present in the hydrothermal alteration zones of porphyry systems (Sinclair, 2007; Sillitoe, 2010). The "green rock environment" is defined as the hydrothermal alteration halo that surrounds porphyry Cu mineralization and is characterized by a high abundance of the green minerals: chlorite and epidote (Cooke et al., 2014, 2020; Lee et al., 2020; Orovan and Hollings, 2020). Epidote is present as a replacement product (e.g., after plagioclase or hornblende) or as a direct precipitate of hydrothermal fluids, typically filling fractures and veins. The high proportion of epidote in this "green rock" alteration assemblage is well reflected in regional epidote glacial dispersal trains in till from the Quesnel terrane of south-central British Columbia, which extend over several kilometers down-ice from the Highland Valley Copper, Gibraltar, Mount Polley and Woodjam porphyry Cu deposits (see Hashmi et al., 2015; Plouffe et al., 2016, 2021a, 2022; Plouffe and Ferbey, 2017) (Fig. 1). Given its common presence and large abundance in nearly all known hydrothermal alteration zones of porphyry Cu deposits, and its resistance to glacial processes and post-glacial weathering, epidote is recognized as a valuable indicator mineral for porphyry Cu mineral exploration (Plouffe and Ferbey, 2017; Plouffe et al., 2021a, 2021b, 2022). As such, epidote can be used as an indicator mineral for porphyry Cu mineralization in detrital sediments (e.g. till and stream sediments), and in particular, enhances exploration for new mineral resources in glaciated terrains (Plouffe and Ferbey, 2017).

In addition to its presence in hydrothermal alteration zones of porphyry deposits, epidote occurs in metamorphic rocks from upper zeolite to intermediate amphibolite facies but is particularly common in greenschist facies rocks (Grapes and Hoskin, 2004). It is present in the Nicola Group rocks of south-central British Columbia where post-mineralization regional burial metamorphism reached zeolite facies at Mount Polley and Woodjam, and greenschist facies at Gibraltar (Greenwood et al., 1991; Panteleyev et al., 1996). Furthermore, the composition of epidote, namely its As and Sb

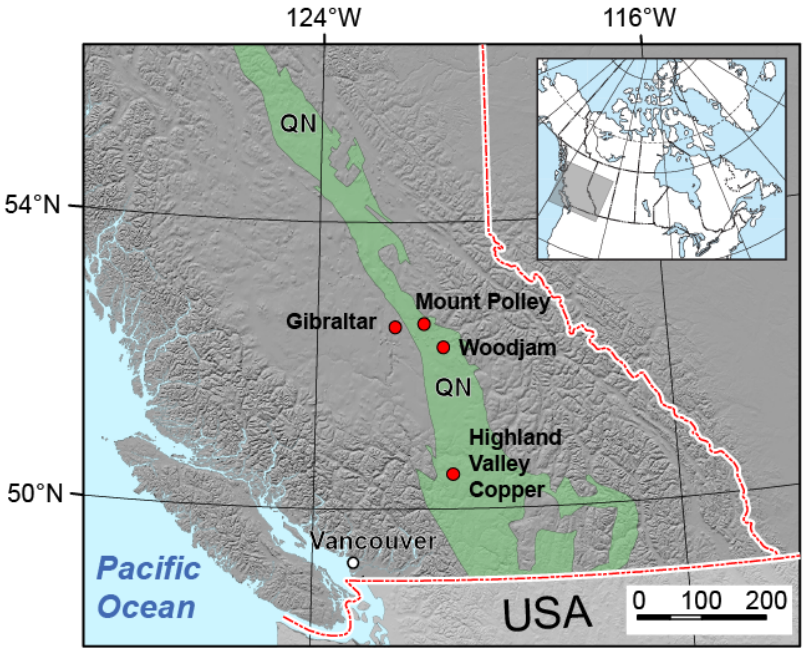

Figure 1. Location of four porphyry Cu study sites in British Columbia mentioned in the text. QN – Quesnel terrane.

contents, can be used to distinguish porphyry-related from metamorphic epidote. Typically, porphyry-related epidote contains approximately >4 ppm As and >0.6 ppm Sb, as opposed to metamorphic epidote which generally contains much lower concentrations of these two elements, commonly below or near LA-ICP-MS detection limits (Baker et al., 2020; Cooke et al., 2020; Plouffe et al., 2021a).

Bedrock and till samples were collected at three porphyry Cu study sites of south-central British Columbia: Gibraltar, Mount Polley and Woodjam (Fig. 1). These deposits are hosted in Late Triassic to Early Jurassic felsic to mafic intrusive rocks that intruded the Upper Triassic Nicola Group succession of island arc volcanic and sedimentary rocks (del Real et al., 2020; Rees et al., 2020; van Straaten et al., 2020). The Nicola Group represents the dominant constituent of the Quesnel terrane. The intrusions hosting porphyry mineralization include the Granite Mountain batholith at Gibraltar, the Mount Polley Intrusive Complex at Mount Polley and the Takomkane batholith and satellite intrusions at Woodjam (Fig. 2).

Methods

Thick polished sections (75 µm) were prepared from the nine bedrock samples. Epidote grains from till were picked from the 0.25-0.50 mm sized fraction of the heavy mineral concentrates (> 3.2 specific gravity) of the samples collected near the Gibraltar and Mount Polley porphyry Cu deposits (Fig. 2). The heavy mineral separation procedures are outlined in Plouffe and Ferbey (2016). The heavy mineral separation and grain picking were completed at Overburden Drilling Management Limited, Ottawa, ON. The grains were mounted in epoxy pucks and polished at IOS Services Geoscientifique Inc., Chicoutimi, QC.

The epidote samples from the intrusive rocks at each of the three study sites were selected because of their high Cu (20 – 500 ppm), As (14 – 205 ppm), or Sb (3 – 870 ppm) concentrations as revealed by LA-ICP-MS spot analysis and reported by Plouffe et al. (2021a). Only one bedrock sample from Mount Polley contains visible Cu mineralization (chrysocolla in sample 18PMA001). Two samples from the Nicola Group (GBR49 and 15PSC22; Fig. 2) were

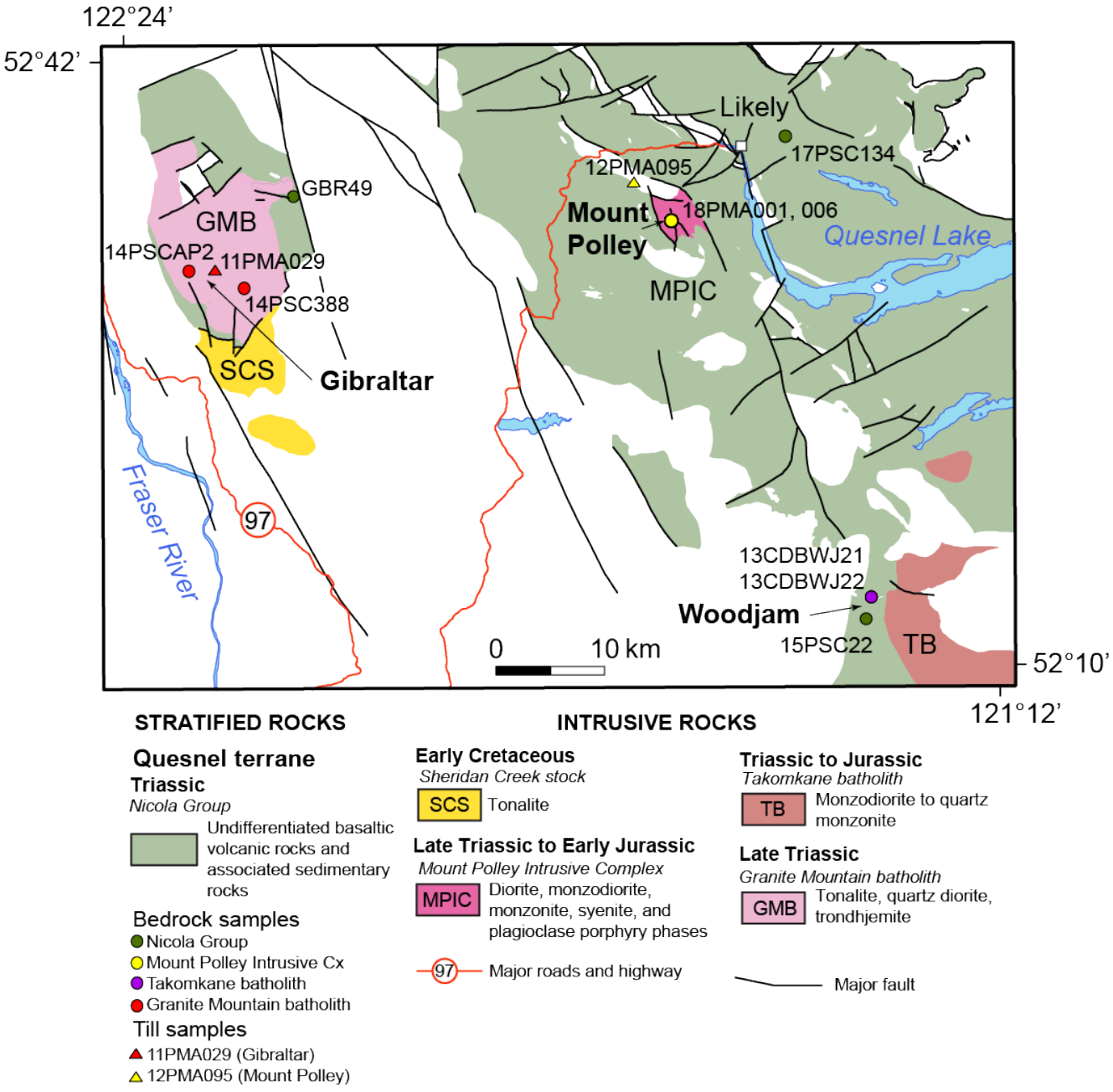

Figure 2. Location map of bedrock and till samples from which epidote was mapped by LA-ICP-MS. Regional geology from Cui et al. (2017).

selected based on their close proximity (<2 km) from the intrusion host of porphyry mineralization at Gibraltar and Woodjam and their high As (12 – 414 ppm) and Sb (4 – 338 ppm) concentrations (Plouffe et al., 2021a). The high As and Sb content of epidote in these Nicola Group rocks could be an indication that it formed as a porphyry-related hydrothermal alteration mineral and not during regional metamorphism (Plouffe et al., 2021a). One sample of epidote from a pyroclastic rock of the Nicola Group collected approximately 12 km northeast of Mount Polley (17PSC134; Fig. 2), and containing low concentrations of As (0.6 – 1.8 ppm) and moderate concentrations of Sb (1.2 – 4 ppm), was selected as it is interpreted to

represent a baseline for metamorphic epidote, with no nearby sources of porphyry-related hydrothermal fluids. Lastly, epidote grains from two till samples (11PMA029 and 12PMA095; Fig. 2) were selected because of their proximity or down-ice location from porphyry mineralization and hydrothermal alteration zones, and their high Cu (5 – 45 ppm), As (3 – 55 ppm), or Sb (3 – 89 ppm) content reported by Plouffe et al. (2021a).

Backscattered electron (BSE) images of epidote were obtained at the Geological Survey of Canada with a TESCAN Mira3 field emission scanning electron microscope (SEM) under the following operating conditions: working distance of 15 nA, accelerating voltage of 20 kV and probe current of 0.4 to 1 nA. The approximate Fe and Al content of epidote was determined by energy dispersive spectrometry (EDS) with an Oxford Industries X-MAX 80 silicon drift detector and the Aztec 5.0 microanalysis software. The acquisition time was 3 s per spot analysis.

Quantitative geochemical mapping of epidote by LA-ICP-MS was completed on the regions of interest of thin sections with dimensions of about 1.5 mm^2. Analyses were done using a Photon Machines/Teledyne Analyte G2 193 nm excimer laser ablation system, with a Helex two-volume ablation cell, coupled to an Agilent 7700x quadrupole ICP-MS. The mapping procedure closely follows the method of Lawley et al. (2015, 2020) and Paradis et al. (2022). Element maps were constructed by translating the sample stage under a focused laser beam, to form a series of raster line scans. Laser conditions during the analytical sessions include: a fluence of 5-6 J/cm^2, a repetition rate of 30 Hz, a spot size of 5 to 8 µm, and a scan speed of 5 to 8 µm/s. The spot size and scan speed were selected such that the sample stage would advance one equivalent spot diameter every 1 second. Prior to each ablation pass, the sample surface was cleaned by passing the laser across the sample at a rate of 2–3 pulses every equivalent spot diameter. The cleaning pass was followed by up to 40 s of washout, then each analysis began with 20 s of background measurement (gas blank). The ablation aerosol was transported out of the Helex cell using ~1 L/min of helium gas and carried to the ICP-MS through ~1 m of 2 mm (inner diameter) Teflon tubing with no SQUID device attached. The total duty cycle time to measure all masses on the ICP-MS (in time-resolved analysis mode) was 250 ms, which allowed for four full scans of the mass spectrometer every 1.0 s (the equivalent of one spot diameter along the line scan). During data processing, these 4 scans were averaged to form one pixel/data point along the line. Dwell times were optimized based on expected count rates in epidote and its host matrix minerals and the natural abundance of the specific isotope used in the acquisition method, such that Ca, Al, Si and other expected major and minor elements in the sample were measured for 2 – 4 ms, and trace elements for 4 – 14 ms (e.g., Cu, As, Sb).

The calibration procedures of Jackson (2008a) were followed during the mapping sessions. Standardization was achieved by calibrating the signals of unknowns against analyses of GSE-1G (for most major and trace elements) (Guillong et al., 2005), and in-house reference materials pyrrhotite (sulphur calibration) and calcite (carbon calibration – where necessary), and normalizing total element (or element oxide) concentrations to 100% on a pixel-to-pixel basis (see Halicz and Günther, 2004). Reference materials were analyzed every 20 unknowns (approximately every hour) to account for instrument drift – which was monitored through analyses of NIST-612. Reference values for GSE-1G and NIST-612 are taken from the online geological and environmental reference materials database (GeoReM) (Jochum et al., 2005). The software programs Lamtrace and Pixelate (Jackson, 2008b) were used to calibrate the data and convert the line scan profiles to quantitative elemental maps. Raw count rates for the individual Pb isotopes were summed prior to calibration, such that a Total Pb concentration could be calculated. The concentration for each of the three individual Pb isotopes was determined by comparing against the isotopic abundance of Pb in GSE-1G. Two-dimensional element concentration maps were constructed

with logarithmic and percentile colour scanning functions using an in-house (GSC) Python script.

Isotopes measured include: ^{23}Na, ^{25}Mg, ^{27}Al, ^{29}Si, ^{31}P, ^{34}S, ^{39}K, ^{42}Ca, ^{45}Sc, ^{47}Ti, ^{51}V, ^{53}Cr, ^{55}Mn, ^{57}Fe, ^{59}Co, ^{60}Ni, ^{65}Cu, ^{66}Zn, ^{75}As, ^{88}Sr, ^{89}Y, ^{90}Zr, ^{95}Mo, ^{109}Ag, ^{121}Sb, ^{137}Ba, ^{139}La, ^{140}Ce, ^{141}Pr, ^{147}Sm, ^{151}Eu, ^{157}Gd, ^{163}Dy, ^{167}Er, ^{173}Yb, ^{206}Pb, ^{207}Pb, ^{208}Pb, ^{209}Bi, ^{232}Th, and ^{238}U and are displayed in parts per million (ppm). Total integrated counts (TIC) and ^{13}C were monitored during the sessions and are reported as counts per second (cps). LA-ICP-MS maps for the following elements are reported in their oxide form: Na_2O_3, MgO, Al_2O_3, SiO_2, P_2O_5, K_2O, CaO and TiO_2. Some of the samples contain significant sections of quartz (e.g. 14PSC388), and due to the poor ablation characteristics of this mineral under normal ablation conditions (< 7 J/cm^2), the resulting maps contained sections of pixels with spotty data (or no data at all) which is representative of quartz. Sections of the map that contain quartz should be considered semi-quantitative (whereas the remainder of the map would not be impacted).

Results

Sample location information is provided in Appendix 1. All LA-ICP-MS analytical results are provided in Appendix 2 which include for each sample: 1) individual maps for each element with a logarithmic and percentile scale bar, 2) raw results as table (csv file), 3) petrographic (RL-reflected light; PPL – plain polarized light) and backscattered electron (BSE) images of the area analyzed and 4) a compilation of all LA-ICP-MS maps in a web browser (html) and PowerPoint (pptx) formats.

Following is a brief description of the LA-ICP-MS maps for each sample.

Gibraltar deposit

14PSC388 – This tonalite sample of the Granite Mountain batholith contains epidote in a chlorite veinlet bordering on quartz and altered plagioclase with fine-grained epidote. Note that for this sample the BSE image was taken post LA-ICP-MS mapping and that the laser tracks are visible (Fig. 3A, Appendix 2). Also, note the poor ablation of quartz in the BSE image (Fig. 3A). There is broad oscillatory Fe-Al zoning in the epidote vein as visible in the BSE images (Fig. 3B, C). The bright regions contain on average 11.0 to 12.3 wt% Fe and 11.6 to 12.4 wt% Al as opposed to the darker regions which contain 7.1 to 7.4 wt% Fe and 14.4 to 14.8 wt% Al as determined by energy dispersive spectroscopy (EDS) in the SEM. Several elements including Sc, Ti, V, Sr, Y, Zr, Sb, REE, and U follow the Fe-Al zoning in epidote with higher concentrations corresponding to high Fe content (brighter regions in BSE images) (Fig. 3 B-E and Appendix 2). Arsenic, Mo and Ag occur in low concentrations with no visible zoning (Appendix 2). Copper shows a net-textured distribution and appears to have been introduced at a late stage along fractures and grain boundaries visible in Figures 3B, C and F.

14PSCAP2 – This second sample of tonalite from the Granite Mountain batholith contains fine grained epidote intergrown with quartz, plagioclase and chlorite (Fig. 4). Titanite inclusions are also present. Vanadium, Sr, Y, REE and U are generally zoned with higher concentrations in the core compared to the rim of epidote (Fig. 4 D, E). Copper and Sb are spotty and heterogeneously distributed in epidote. Cu occurs in higher concentrations in chlorite compared to epidote. Measured concentrations of As, Ag and Mo are very low.

Mount Polley

18PMA001 – In this Cu mineralized sample of a vein within a hydrothermal breccia of the Mount Polley Intrusive Complex, coarse pale yellow green epidote is intergrown with chrysocolla. Epidote in this sample is characterized by complex Fe-Al zoning visible in the BSE images (Fig. 5). Variations in Ti, V, As, Sb and Pb contents generally follows the Fe-Al zoning observed in the BSE images, with higher concentrations typically associated with high Fe content (Fig. 5B to D and Appendix 2). Conversely, high Mn occurs in growth zones that are generally associated with high Al contents (Fig. 5B to F and Appendix 2). Copper, Zn, Zr and REE are elevated along the rims and the

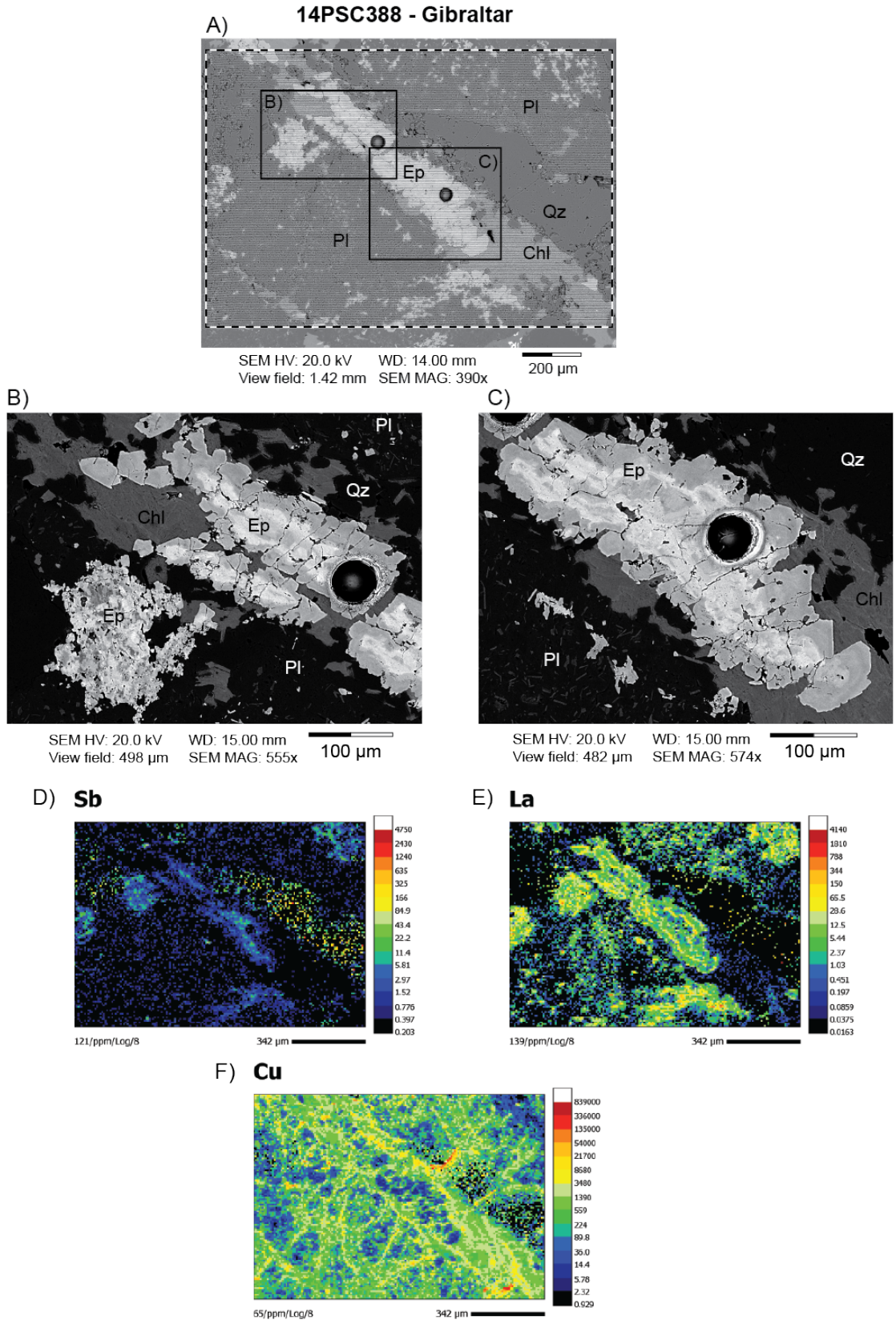

Figure 3. BSE image of sample 14PSC388 from a tonalite of the Granite Mountain batholith at Gibraltar. The dashed line in A) shows the extent of the LA-ICP-MS maps in Appendix 2. B) and C) are detailed views of the epidote. Note the poor ablation of quartz in A). D), E) and F) are examples of LA-ICP-MS maps (Sb, La and Cu). Chl – chlorite, Ep – epidote, Pl – plagioclase, Qz – quartz.

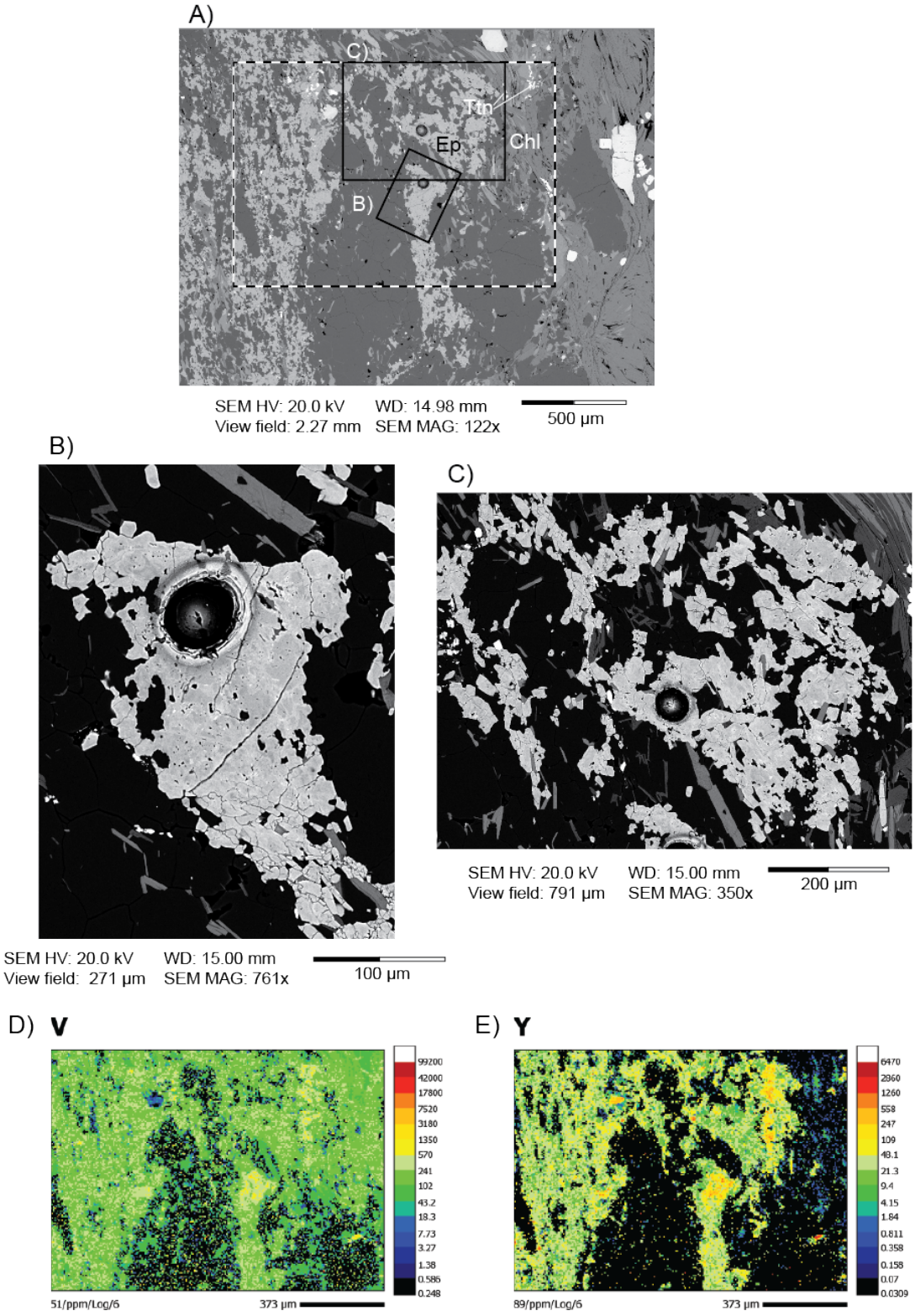

Figure 4. BSE image of sample 14PSCAP2 from epidote in a tonalite of the Granite Mountain batholith at Gibraltar. The dashed line in A) shows the extent of the LA-ICP-MS maps in Appendix 2. B) and C) are detailed views of the epidote. D) and E) are examples of LA-ICP-MS maps (V and Y). Chl – chlorite, Ep – epidote, Ttn – titanite.

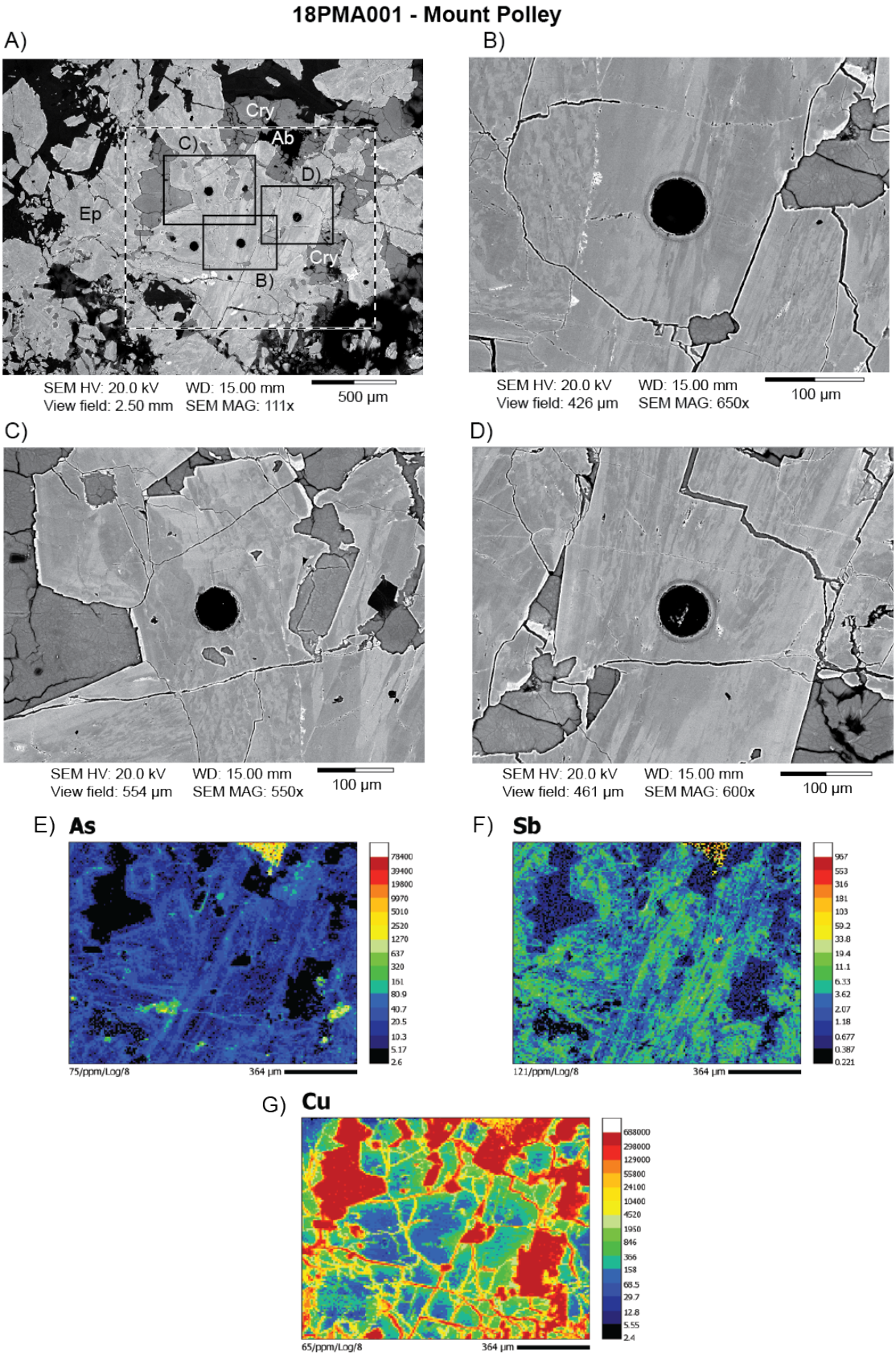

Figure 5. BSE image of sample 18PMA001 from an epidote veinlet in hydrothermal breccia of the Mount Polley Intrusive Compex. The dashed line in A) shows the extent of the LA-ICP-MS maps in Appendix 2. B), C) and D) are detailed views of the epidote. E), F) and G) are examples of LA-ICP-MS maps (As, Sb, Cu). Ab – albtie, Cry – chrysocolla, Ep – epidote.

fractures compared to the core of epidote (Fig. 5G and Appendix 2). Molybdenum and Ag occur in low concentrations with no visible patterns.

18PMA006 – This is a sample of an epidote veinlet in a hydrothermal breccia of the Mount Polley Intrusive Complex. As for sample 18PMA001, epidote in this sample is characterized by complex Fe-Al zoning in the BSE images (Fig. 6). High concentrations of As, Sr, Y, Sb, and REE occur in annealed fractures in epidote, which appears to cross-cut primary Fe-Al growth zoning (Fig. 6B to D, F and Appendix 2). The highest Ti concentrations correspond to titanite inclusions (Fig. 6A-E).

Woodjam

13CDBWJ21 – This sample of monzonite contains fractures infilled with epidote and tourmaline. The distribution of Mg, K, Cu, Zn and Ba is controlled by the presence of fractures in epidote (Fig. 7A-E) which suggests late enrichment of these elements via infiltration of fluids. High P and Mn concentrations generally occur in Al-rich growth zones, as opposed to high Ti, Y, Sb, REE, Yb, Bi, Th and U contents which are associated with Fe-rich growth zones (Fig. 7B and Appendix 2). The distribution of Sc, As, and Zr generally follows Fe-Al growth zoning but the correlation between these trace and major elements is irregular (Fig. 7B and Appendix 2). The presence of heterogeneous P concentrations in epidote without the presence of apatite or other phosphorous mineral phase is only observed in the two samples from Woodjam: 13CDBWJ21 and 13CDBWJ22 (see below).

13CDBWJ22 – This sample of a mafic interval within monzonite containing tourmaline and pyrite veins with epidote shows similar heterogeneous distribution patterns of P, Sc, Ti, V, Mn, Cu, As, Y, Zr, Sb, Ba, REE, Pb, Th and U in epidote as observed in the previous sample. Thorium is elevated in LREE rich zones. No BSE image is available for this sample in Appendix 2.

Nicola Group

GBR49 – This is a sample of Nicola Group mafic volcanic rock collected near the Granite Mountain batholith at Gibraltar. The LA-ICP-MS map was completed on a yellow-orange to red epidote vein from this sample. The boundary of individual epidote crystals shows a high brightness in the BSE images of Figure 8B and C, which could be related to Fe-rich growth zoning. Some crystals show zoning with increasing brightness from inner to outer portions of individual crystals. However, the spatial resolution of the LA-ICP-MS maps is not sufficient enough to discriminate specific element zoning within these individual crystals.

Iron-Al zoning parallel to the vein walls are visible in the BSE images (Fig. 8B, C). Scandium, Ti, V, Sr, Y, REE, Th, and U are generally concentrated in Fe-rich growth zones (Fig. 8A-F). On the other hand, As-, Zr- and Pb-rich zones follow the high Al growth bands (Fig. 8G). Antimony generally follows Fe-Al zoning but the correlation between these elements appears inconsistent (Fig. 8G). Spotty zones of high Ti are related to the presence of titanite (Fig. 8B, E).

15PSC22 – A zone of epidote intergrown with actinolite and hematite occurs in a sample of coarse plagioclase porphyry of the Nicola Group near Woodjam (Fig. 9). No clear elemental zoning is observed in the epidote of this sample but there is a heterogeneous distribution of P, Sc, As, Y, Zr, Sb, REE, Th and U. Zones with elevated Sb are not correlated with As (Fig. 9B, C). The trace elements Sc, V, Mn, Y, Sb, REE, Bi, Th, and U occur in higher concentrations in epidote compared to actinolite (Fig. 9D and Appendix 2). Conversely, Mn, Co, Ni, Zn, Ba, and Pb are elevated in actinolite relative to hematite and epidote (Fig. 9E and Appendix 2). Exceptionally for this sample, the outline of epidote is depicted in Appendix 2 to better show the distinction between epidote and actinolite.

17PSC134 – This epidote sample is from a pyroclastic rock of the Nicola Group obtained 12 km northeast of the Mount Polley deposit. Given the location of this sample, far from the influence of hydrothermal porphyry alteration, epidote in

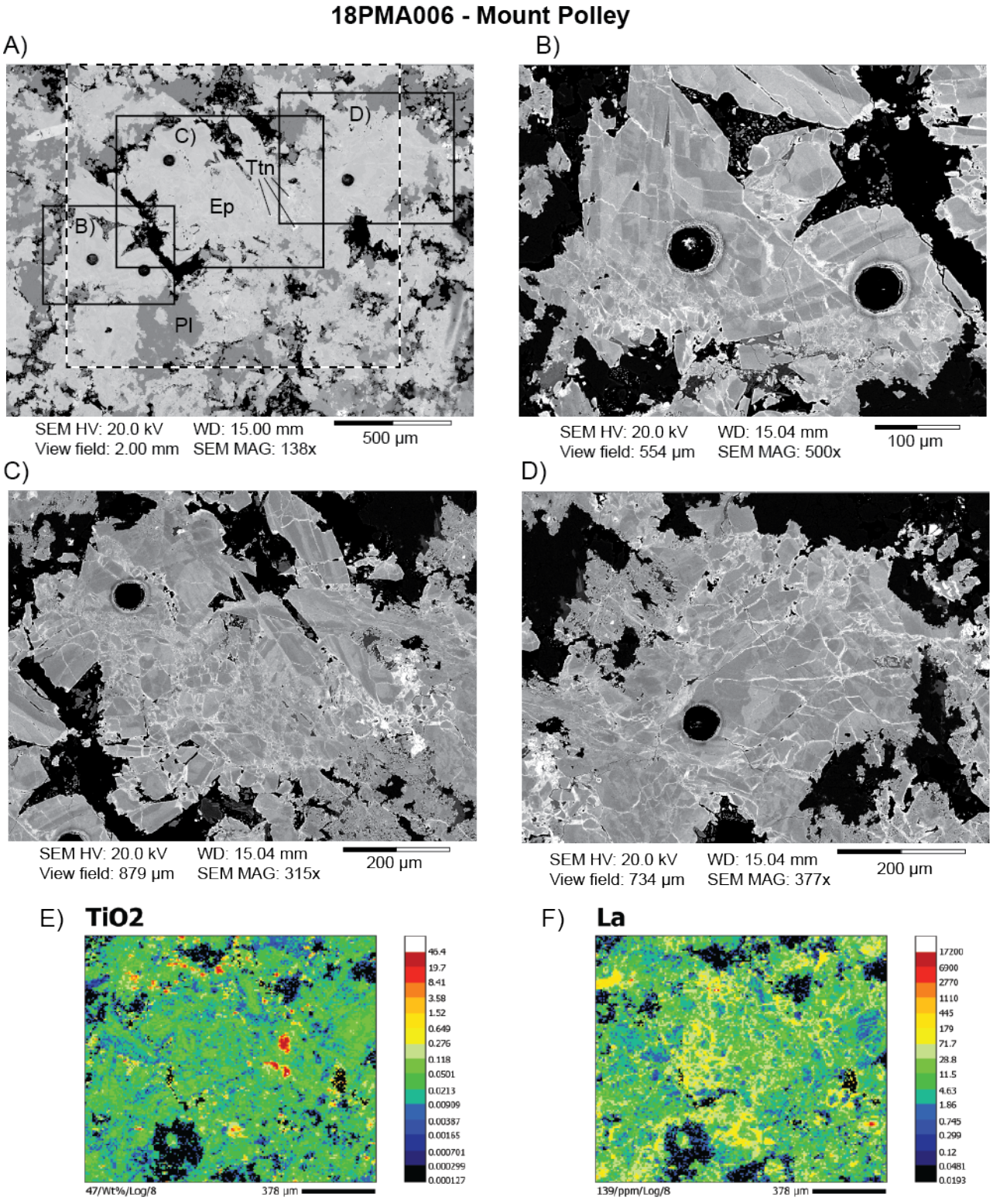

Figure 6. BSE image of sample 18PMA006 from an epidote veinlet in hydrothermal breccia of the Mount Polley Intrusive Compex. The dashed line in A) shows the extent of the LA-ICP-MS maps in Appendix 2. B), C) and D) are detailed views of the epidote. E) and F) are examples of LA-ICP-MS maps (TiO_2 and La). Ep – epidote, Pl – plagioclase, Ttn – titanite.

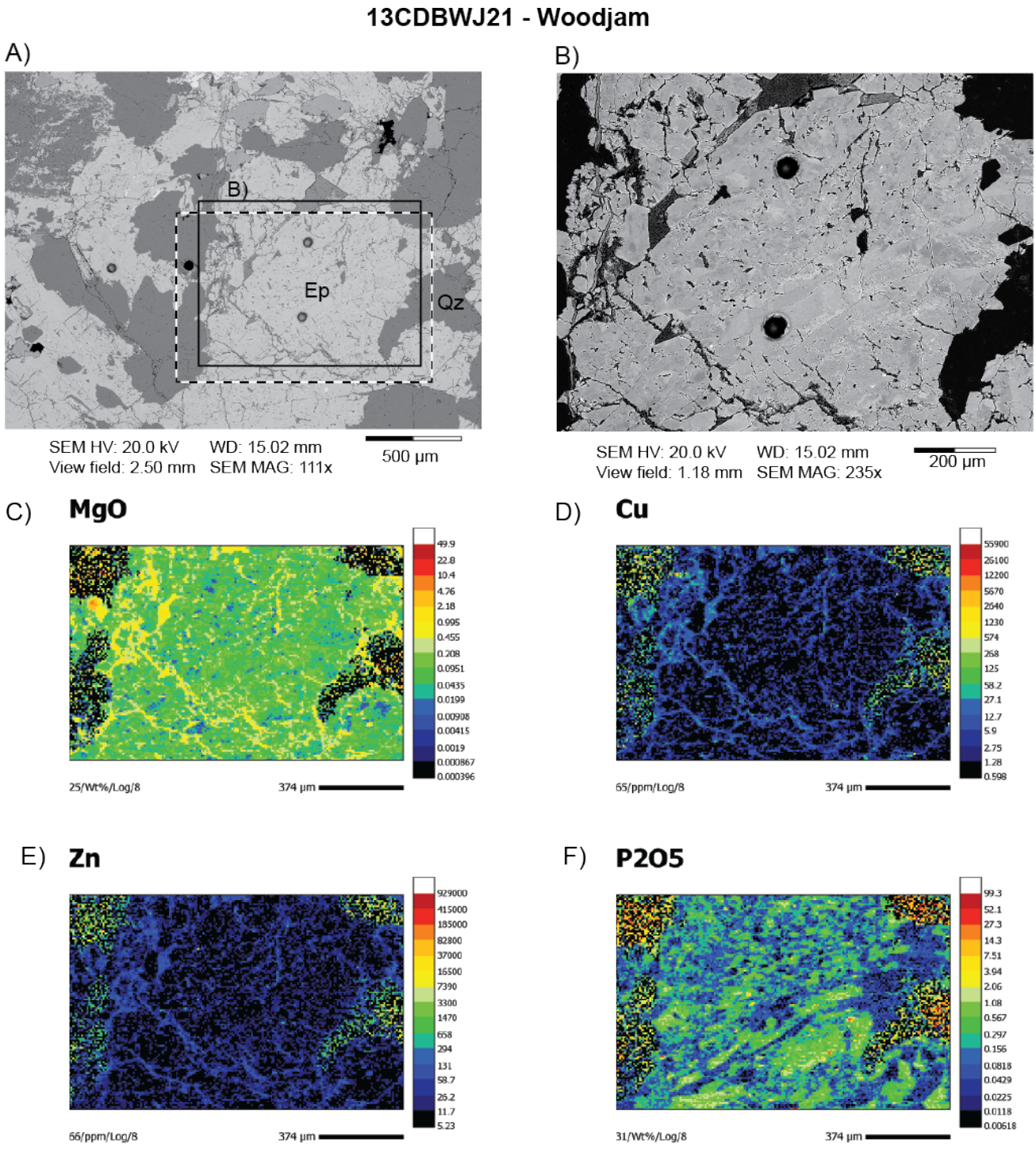

Figure 7. BSE image of sample 13CDBWJ21 from a monzonite at Woodjam with epidote replacing plagioclase intergrown with quartz. The dashed line in A) shows the extent of the LA-ICP-MS maps in Appendix 2. B) is a detailed view of the epidote with higher contrast. C), D), E) and F) are examples of LA-ICP-MS maps (MgO, Cu, Zn, P_2O_5). Ep – epidote, Qz - quartz.

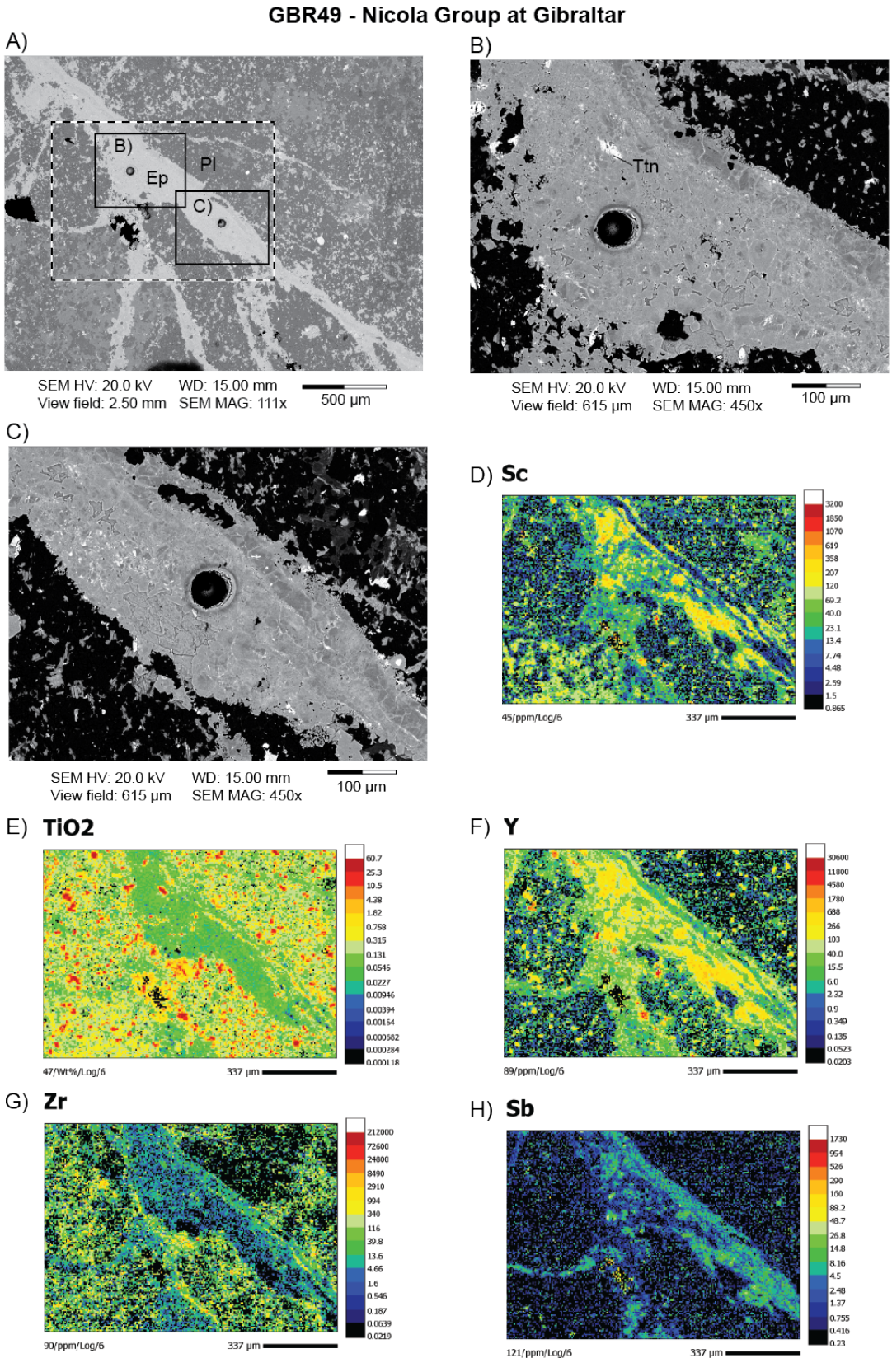

Figure 8. BSE image of an epidote veinlet in sample GBR49 of Nicola Group mafic volcanic rock near the Granite Mountain batholith at Gibraltar. The dashed line in A) shows the extent of the LA-ICP-MS maps in Appendix 2. B) and C) are detailed views of the epidote. D) to H) are examples of LA-ICP-MS maps (Sc, TiO_2, Y, Zr, Sb). Ep – epidote, Pl – plagioclase, Ttn – titanite.

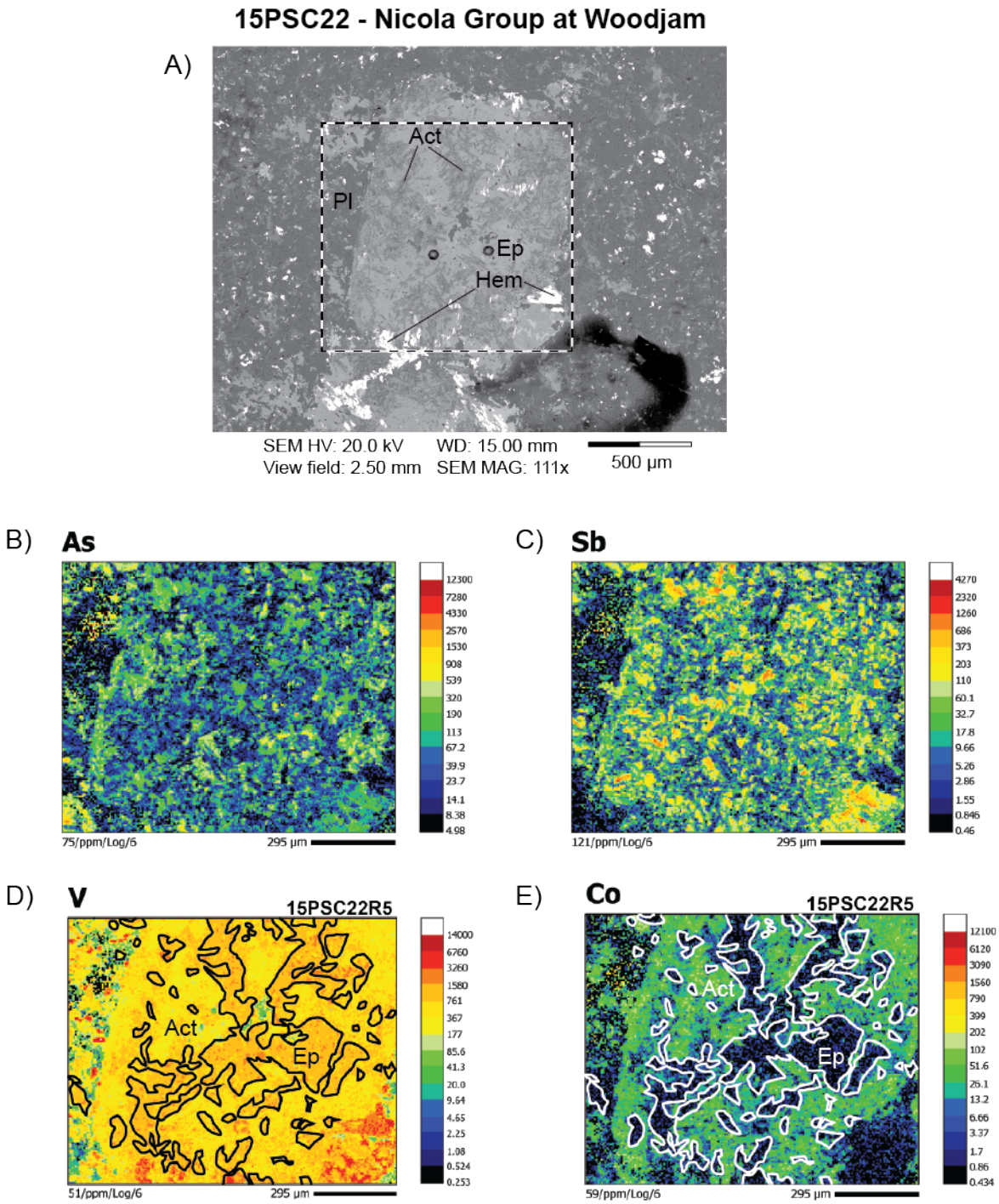

Figure 9. BSE image of epidote in sample 15PSC22 of Nicola Group volcanic rock near Woodjam. The dashed line in A) shows the extent of the LA-ICP-MS maps in Appendix 2. B) to E) are examples of LA-ICP-MS maps (As, Sb, V, Co). The contour of epidote is shown in D) and E) to better show the composition difference between it and actinolite. Act – actinolite, Ep – epidote, Hem – hematite, Pl – plagioclase

this sample is interpreted as metamorphic in origin. This sample contains euhedral poikilitic epidote that overprints the matrix. The distribution of epidote in this sample is best illustrated in the Ca map (Fig. 10A, D). No clear Fe-Al zoning is visible in the BSE images (Fig. 10B, C). The trace elements Sc, V, Sr, Y, Zr, Sb, REE, and Pb have higher abundances in epidote – with some of these elements (Sc, Cu) elevated along grain boundaries and fractures – compared to the surrounding matrix (Fig. 10E, F). Higher concentrations of Co, Ni, Cu, and Zn occur in the matrix compared to epidote (Fig. 10E). Arsenic concentrations are low but Sb high concentration speckles are present in epidote.

Epidote grains from till

All the grains from till show Fe-Al zoning in BSE – similar to the bedrock samples (Fig. 11-14). Geochemical characteristics specific to each grain are described below.

11PMA029_gr1 – In this first epidote grain from a till sample collected 1 km northwest of the Gibraltar deposit (11PMA029, Fig. 2), most elements are homogeneously distributed except for Y and light REE, which show similar linear distribution patterns not consistent with Fe-Al zoning (Fig. 11A, B). Also, isolated clusters of Sb are present (Fig. 11A, C). There are several suspected chlorite inclusions about 10 µm in size based on the MgO and Fe maps (Fig. 11D, E). Copper-rich inclusions of an unknown mineral are also present (Fig. 11F). The nature of the high concentrations of K and Ba along the rim of epidote is uncertain (Fig. 11G, H). It could be related to a pedogenetic precipitate. It is unlikely a primary characteristic of the epidote preserved after glacial erosion and comminution.

11PMA029_gr2 – This second epidote grain from till sample 11PMA029 from the Gibraltar region (Fig. 2) contains several inclusions of a Ti-rich mineral which occur as bright zones in BSE and warm colors in the TiO_2 map (Fig. 12A, B). The Ti-rich inclusions contain high Cu but low Y compared to epidote (Fig. 12C, D). These mineral inclusions are most likely rutile as also identified in bedrock samples from the Gibraltar deposit (Kobylinski et al., 2016). Elevated Sc and REE contents occur as a distinct zone in the lower right sector of the grain (Fig. 12E, F).

12PMA095_gr1 – This first epidote grain from till sample 12PMA095, collected 5 km northwest of the Mount Polley deposit, contains a homogeneous distribution of elements except for As, Sb, La, Ce, and Pr, and to a lesser extent Eu, Th and U, which are elevated in a distinct zone on the right side of the grain (Fig. 13 B, C). Chlorite (high MgO and low CaO) is attached to this epidote grain and titanite inclusions are visible in the BSE image (bright zones) and the TiO_2 map (Fig. 13A, D-F). Titanite contains, in addition to Ti, higher concentrations of V, Y, REE, Th and U compared to epidote (Fig. 13F, G). Phosphate inclusions (apatite?) are also identified in the P_2O_5 map (Fig. 13H).

12PMA095_gr2 – Arsenic, Y, and especially Sb are concentrated in a distinct zone on the left portion of the grain, and are correlated with a Fe-rich band in the BSE image (Fig. 14A-C). Other elements are homogeneously distributed in epidote. This epidote grain contains biotite (and chlorite?) as shown from the K_20 map (Fig. 14A, D). Titanium, Co, Cu, Zn, and light REE (La, Ce, Pr) are higher in abundance in biotite compared to epidote (Fig. 14, E, F, G).

Discussion

Major elements in epidote

Irregular Al-Fe zoning in epidote occurs as mottled and complex patterns in BSE images (Fig. 3 to 12) and is visible in some of the geochemical maps (Appendix 2). Only in sample 17PSC134 was the Fe-Al zoning not observed (Fig. 10). This sample is interpreted to contain principally metamorphic epidote given its distal location (12 km) from the nearest porphyry mineralized centre. The absence of Fe-Al zoning in epidote of this sample is not necessarily indicative of metamorphic epidote. Franz and Liebscher (2004) and Grapes and Hoskin (2004) both report the presence of Fe-Al zoning in metamorphic epidote in some cases, with Fe-rich core and Al-rich rim zones reflecting a transition from sub-greenschist conditions evolving to higher metamorphic grades. But numerous

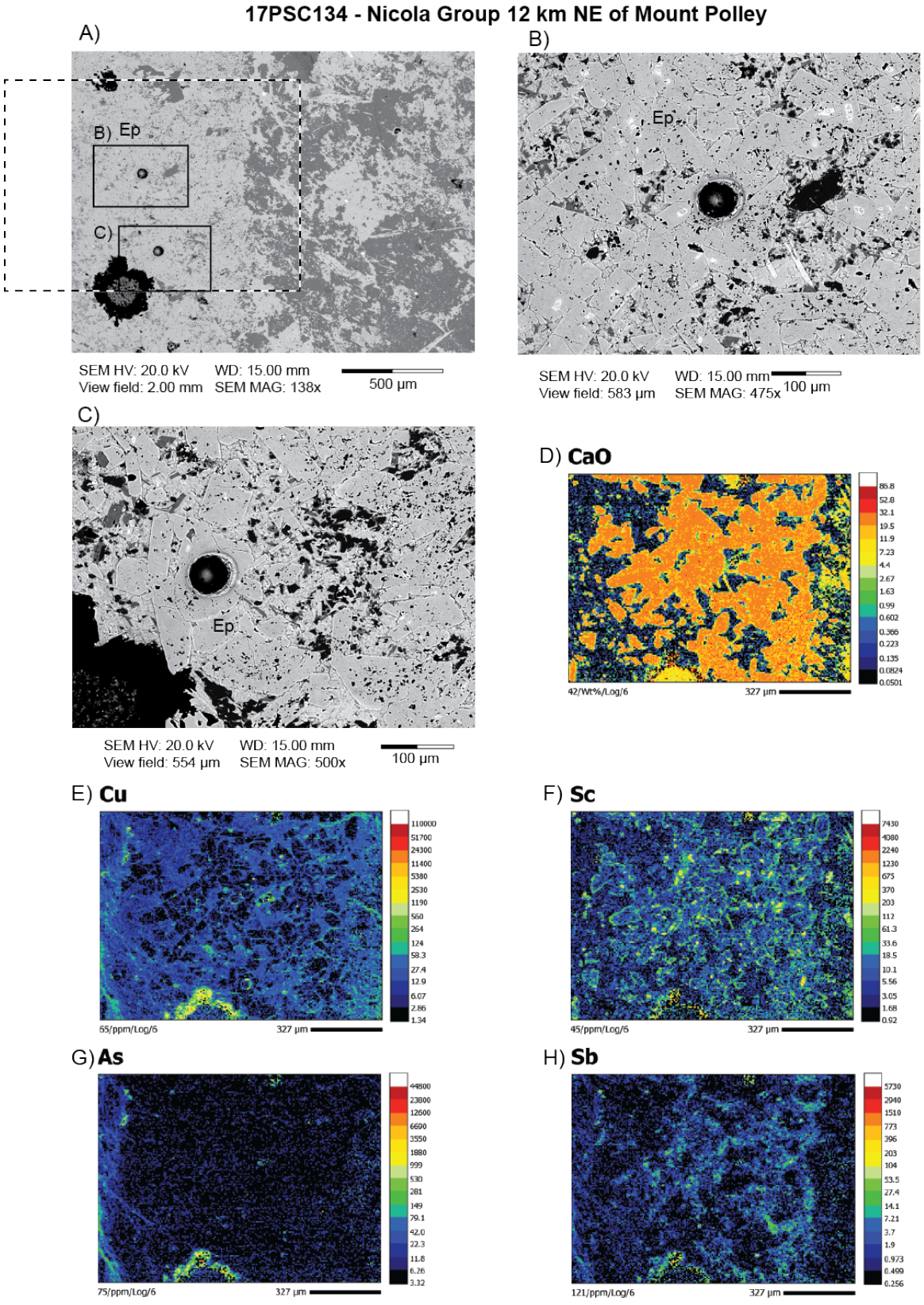

Figure 10. BSE images of epidote in sample 17PSC134 of a pyroclastic bedrock of the Nicola Group obtained at 12 km northeast of the Mount Polley. The dashed line in A) shows the extent of the LA-ICP-MS maps which extend outside of the field of view A). B) and C) are detailed views of the epidote. Note the absence of Fe-Al zoning in the epidote. D) to H) are examples of LA-ICP-MS maps (CaO, Cu, Sc, As, Sb).

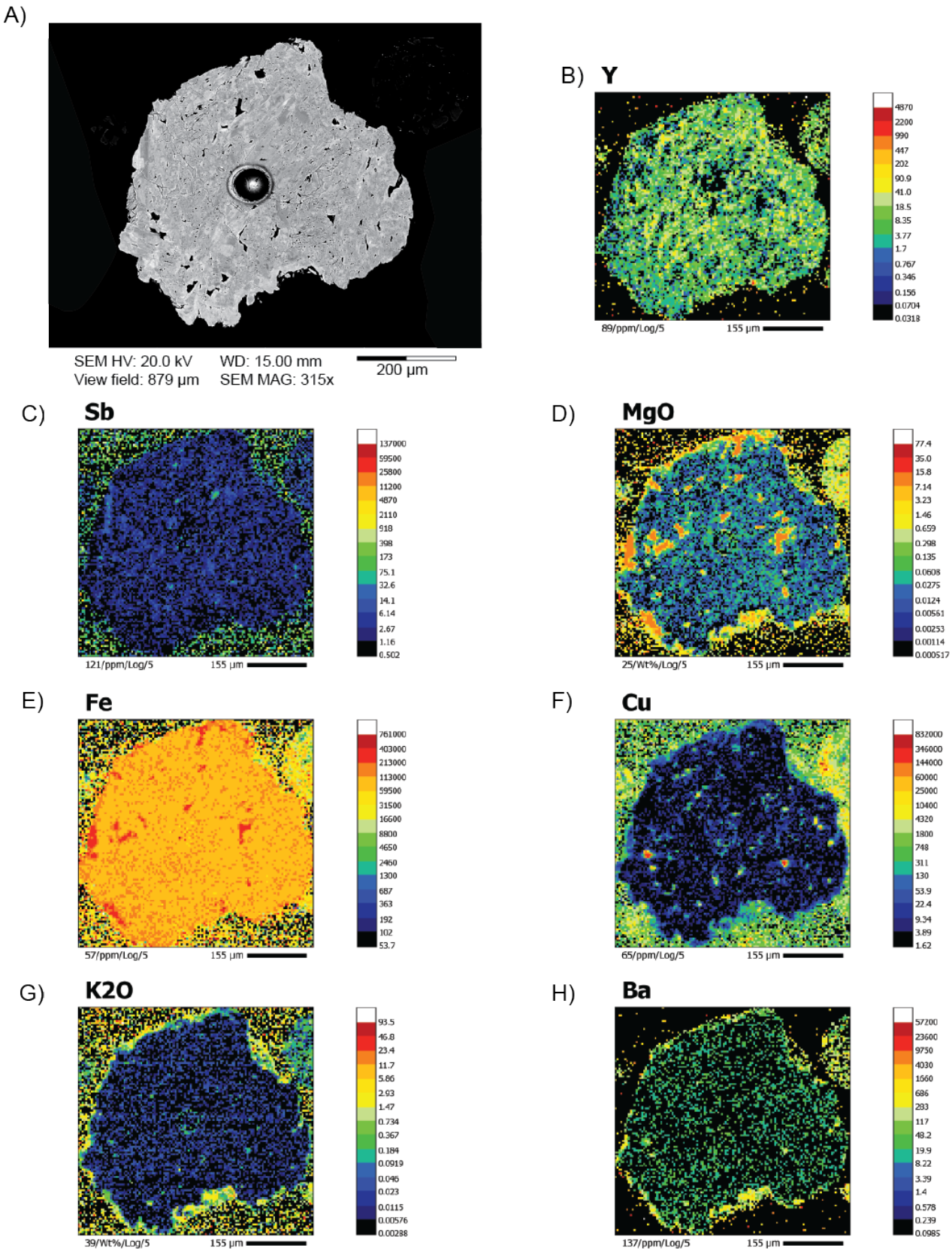

Figure 11. A) BSE image of an epidote grain (grain 1) from till sample 11PMA029 at Gibraltar. B) to H) are examples of LA-ICP-MS maps (Y, Sb, MgO, Fe, Cu, K_2O, Ba).

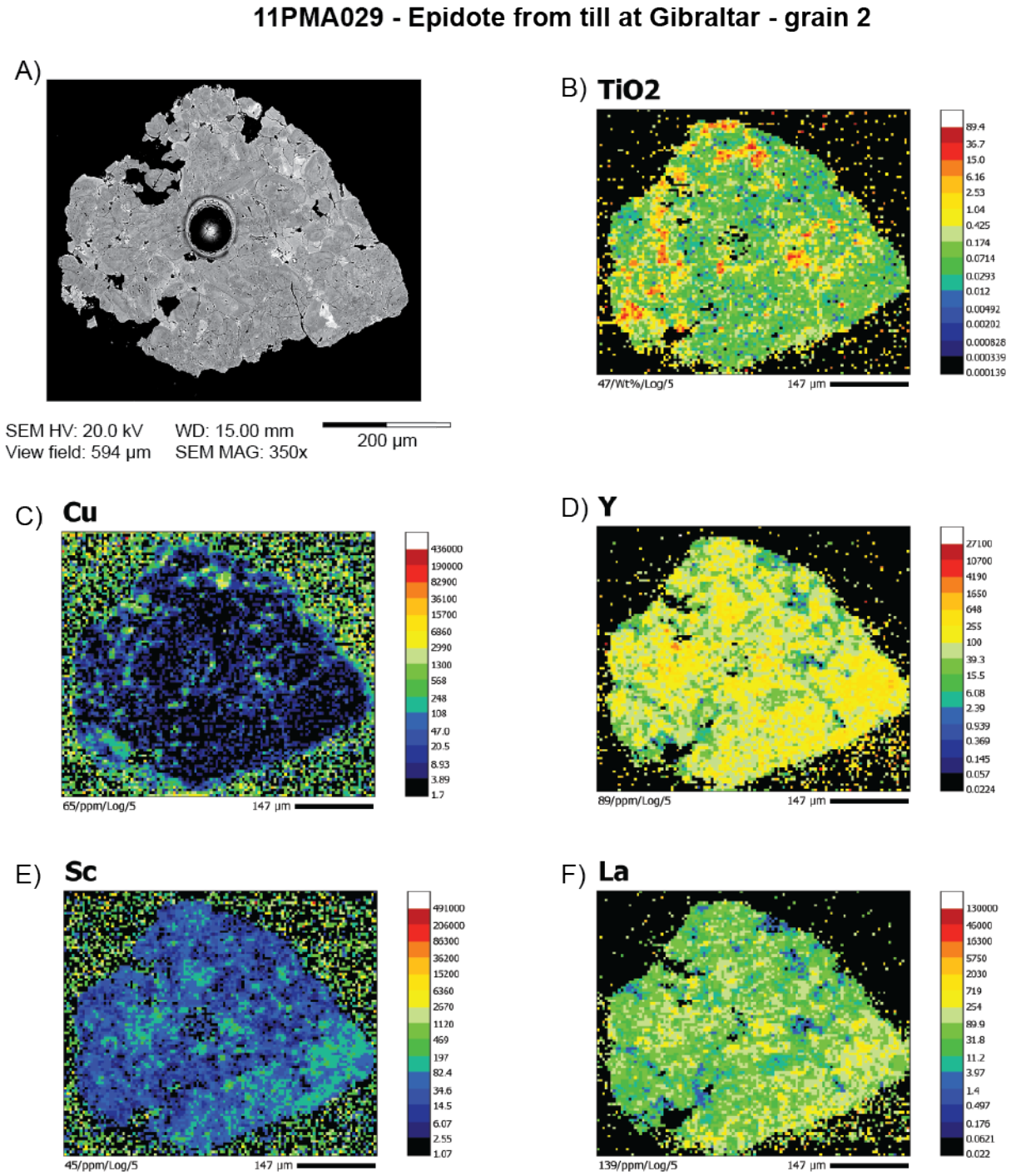

Figure 12. A) BSE image of an epidote grain (grain 2) from till sample 11PMA029 at Gibraltar. B) to F) are examples of LA-ICP-MS maps (TiO_2, Cu, Y, Sc, La).

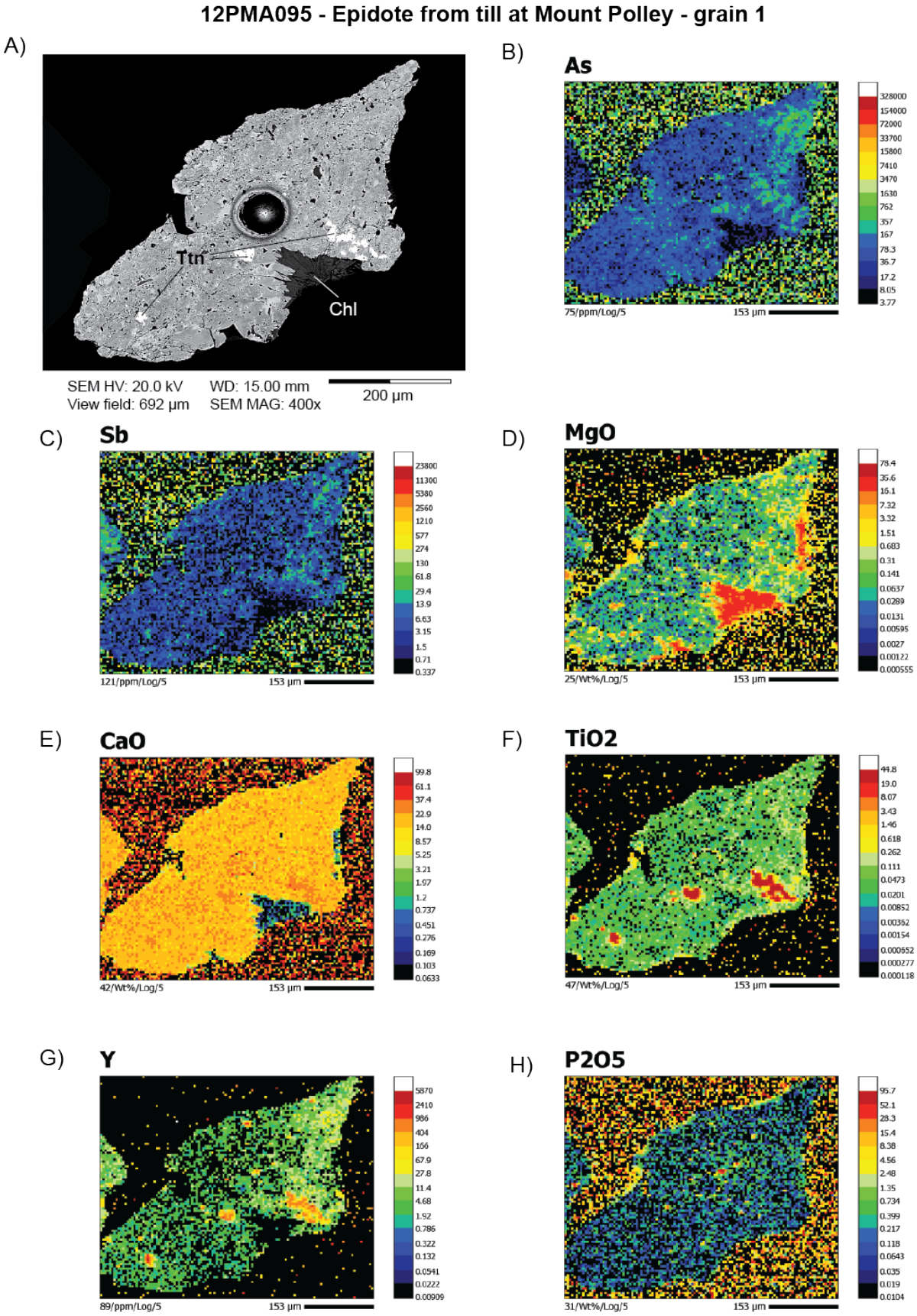

Figure 13. A) BSE image of an epidote grain (grain 1) from till sample 12PMA095 at Mount Polley. B) to H) are examples of LA-ICP-MS maps (As, Sb, MgO, CaO, TiO_2, Y, P_2O_5). Chl – chlorite, Tnt – titanite

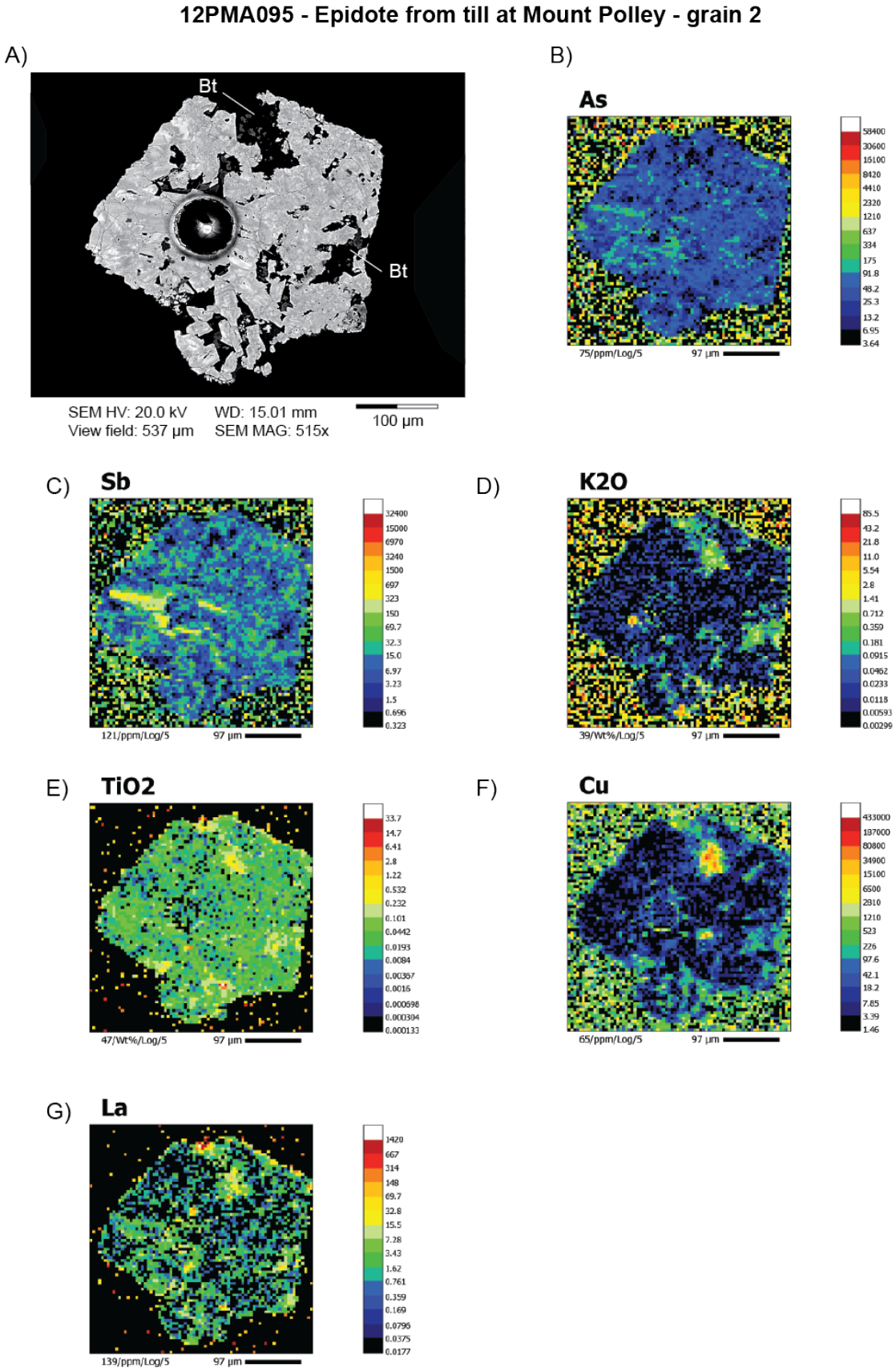

Figure 14. A) BSE image of an epidote grain (grain 2) from till sample 12PMA095 at Mount Polley. B) to G) are examples of LA-ICP-MS maps (As, Sb, K2O, TiO_2, Cu, La). Bt – biotite

exceptions to this general zoning trend are also noted by these authors. Nonetheless, the textural difference we observe in Fe-Al zoning between porphyry- and metamorphic-related epidote from British Columbia will need to be followed up with thorough additional testing, as major element zoning patterns could be a preliminary indicator for porphyry-related epidote.

Trace elements in epidote

In addition to major elements, a number of trace elements (Mg, P, K, Sc, Ti, V, Mn, Cu, Zn, As, Y, Zr, Sr, Y, Sb, Ba, REE, Pb, Bi, Th, U) are variably distributed in epidote and follow the broad textures of Fe-Al zoning (Figs. 3, 5, 7, 14). Most of these elements occur in higher concentrations in the Fe-rich zones of epidote (high brightness in BSE images) except for Mn and P in sample 13CDBWJ21 from Woodjam (Fig. 7) and As, Zr and Pb in sample GBR-49 from Gibraltar (Fig. 8). However, the correlation between the distribution of trace elements and Fe-Al zoning is not always clear given the lower resolution of the LA-ICP-MS geochemical maps compared to the BSE images.

Elemental zoning from the inner to outer portions of individual epidote crystals is observed in some of the epidote (e.g. Figs. 3, 8). The compositional zoning in epidote could result from variable conditions during crystal growth (e.g. oxidation state, pH, oxygen fugacity, and change in fluid composition, temperature and pressure; Holdaway, 1972; Grapes and Hoskin, 2004). Zoning can also be controlled by the presence of co-crystalizing mineral phases (Holdaway, 1972) or can result from the preferential elemental concentrations along certain faces during crystal growth (Enami et al., 2004).

Lastly, we note the occurrence of high Cu, Zn, and REE abundances along fractures in epidote (Figs. 3F, 5G, 6F, and 10E, F), which are interpreted to be due to the late infiltration of hydrothermal fluids. In sample 18PMA001, these fluids are responsible for the formation of chrysocolla and the high Cu and REE concentrations along the rims and decreasing toward the core of epidote (Fig. 5A, G).

Implications for epidote composition assessment

The observed compositional zoning and heterogeneous elemental distribution in epidote as revealed by LA-ICP-MS mapping shows that there is considerable intra-grain variability in the elemental distribution in this mineral, likely due to the complex hydrothermal environment it forms in, which needs to be considered in the application of geochemical fingerprinting of potential epidote sources in mineral exploration. This includes the identification of epidote potentially derived from a porphyry hydrothermal system based on their As and Sb contents or the evaluation of the fertility potential of a hydrothermal system based on Cu contents (Plouffe et al., 2021a, 2022). The internal chemical variability in epidote can be offset by using a large laser spot size (> 50 µm) and assessed by conducting multiple LA-ICP-MS spot analyses per sample. For example, Ahmed et al. (2020) suggest to conduct about 40 LA-ICP-MS spot analysis per sample of vein epidote to obtain a statistically reliable average value if the data set is to be used to vector towards mineralization as shown by Byrne (2019), Baker et al. (2020), Cooke et al. (2020) and Wilkinson et al. (2020). Although such a large number of laser sport analyses is possible for rock samples with numerous epidote crystals, it is not applicable for detrital epidote grains in the 0.25–0.50 mm size range on which a maximum of two spot analyses can typically be achieved. Plouffe et al. (2021a, 2022) report that analyzing a total of 60 to 80 epidote grains from seven to nine till samples distributed in the region of a porphyry Cu deposit is sufficient to identify porphyry-related epidote (high As and Sb) within a regional dispersal train.

Conclusion

The microscopic composition of porphyry-Cu related epidote from south-central British Columbia mapped by LA-ICP-MS reveals heterogeneities in the distribution of major (Fe and Al) and trace elements in this mineral. The zoning and heterogeneous distribution of

elements in epidote is thought to be due to variable conditions during crystallization such as changes in oxidation state, pH, oxygen fugacity, fluid composition, temperature and pressure. It can also be caused by the late infiltration of hydrothermal fluids after the crystallization of epidote. Sample size permitting, multiple laser spot analyses should be conducted on epidote to overcome this variability and evaluate its composition as a mineral exploration vectoring tool for porphyry Cu mineralization.

Acknowledgements

This research greatly benefited from samples provided by J.B. Chapman (13CDB's), C.H. Kobylinski (GBR49), C. Rees (18PMA's), and P. Schiarizza (PSC's). This study was supported by the Targeted Geoscience Initiative 6 Program of the GSC. The authors acknowledge and greatly appreciate the direct and indirect support provided by the mine operators and exploration site owners. This open file greatly benefited from the internal GSC review by Riccardo Graziani.

References

Ahmed, A. D., Fisher, L., Pearce, M., Escolme, A., Cooke, D. R., Howard, D., and Belousov, I., 2020, A microscale analysis of hydrothermal epidote: implications for the use of laser ablation-inductively coupled plasma-mass spectrometry mineral chemistry in complex alteration environments: Economic Geology, v. 115, p. 793-811.

Baker, M. J., Wilkinson, J. J., Wilkinson, C. C., Cooke, D. R., and Ireland, T., 2020, Epidote trace element chemistry as an exploration tool in the Collahuasi District, northern Chile: Economic Geology, v. 115, p. 749-770.

Byrne, K., 2019, Diagnostic features of the rocks and minerals peripheral to the Highland Valley Copper district, British Columbia, Canada: Implications for the genesis of porphyry Cu systems and their footprints, The University of Alberta, 211 p.

Cooke, D. R., Baker, M., Hollings, P., Sweet, G., Zhaoshan, C., Danyushevsky, L., Gilbert, S., Zhou, T., White, N., Gemmell, J. B., and Inglis, S., 2014, New advances in detecting the distal geochemical footprints of porphyry systems - epidote mineral chemistry as a tool for vectoring and fertility assessments, *in* Kelley, K. D., and Golden, H. C., eds., Building Exploration Capability for the 21st Century, Special Publication No. 18: Littleton, Colorado, Society of Economic Geologists, p. 127-152.

Cooke, D. R., Wilkinson, J. J., Baker, M., Agnew, P., Phillips, J., Chang, Z., Chen, H., Wilkinson, C. C., Inglis, S., Hollings, P., Zhang, L., Gemmell, J. B., White, N. C., Danyushevsky, L., and Martin, H., 2020, Using mineral chemistry to aid exploration: a case study from the Resolution porphyry Cu-Mo deposit, Arizona: Economic Geology, v. 115, p. 813-840.

Cui, Y., Miller, D., Schiarizza, P., and Diakow, L. J., 2017, British Columbia digital geology British Columbia Ministry of Energy, Mines and Petroleum Resources, 9 plus digital files. p.

del Real, I., Bouzari, F., and Sherlock, R., 2020, The magmatic and hydrothermal evolution of the Woodjam Cu-Au and Cu-Mo porphyry district, central British Columbia, Canada, *in* Sharman, E. R., Lang, J. R., and Chapman, J., eds., Porphyry deposits of the Nortwestern Cordillera of North America: A 25-year update, Special Volume 57, Canadian Institute of Mining, Metallurgy and Petroleum, p. 601-620.

Enami, M., Liou, J. G., and Mattinson, C. G., 2004, Epidote minerals in high P/T metamorphic terranes: subduction zones and high- to ultrahigh-pressure metamorphism: Reviews in Mineralogy and Geochemistry, v. 56, p. 347-398.

Franz, G., and Liebscher, A., 2004, Physical and chemical properties of the epidote minerals - an introduction: Reviews in Mineralogy and Geochemistry, v. 56.

Grapes, R. H., and Hoskin, P. W. O., 2004, Epidote group minerals in low-medium pressure metamorphic terranes: Reviews in Mineralogy and Geochemistry, v. 56, p. 301-345.

Greenwood, H. J., Woodsworth, G. J., Read, P. B., Ghent, E. D., and Evenchick, C. A., 1991, Metamorphism, *in* Gabrielse, H., and Yorath, C. J., eds., Geology of the Cordilleran Orogen in Canada, Geology of Canada, n. 4, Geological Survey of Canada, p. 535-570.

Guillong, M., Hametner, K., Reusser, E., Wilson, S. A., and Günther, D., 2005, Preliminary characterisation of new glass reference materials

(GSA-1G, GSC-1G, GSD-1G and GSE-1G) by laser ablation-inductively coupled plasma-mass spectrometry using 193 nm, 213 nm and 266 nm wavelengths: Geostandards and Geoanalytical Research, v. 29, p. 315-331.

Halicz, L., and Günther, D., 2004, Quantitative analysis of silicates using LA-ICP-MS with liquid calibration: Journal of Analytical Atomic Spectrometry, v. 19, p. 1539-1545.

Hashmi, S., Ward, B. C., Plouffe, A., Leybourne, M. I., and Ferbey, T., 2015, Geochemical and mineralogical dispersal in till from the Mount Polley Cu-Au porphyry deposit, central British Columbia, Canada: Geochemistry: Exploration, Environment, Analysis, v. 15, p. 234-249.

Holdaway, M. J., 1972, Thermal stability of Al-Fe epidote as a function of fO_2 and Fe content: Contributions to Mineralogy and Petrology, v. 37, p. 307-340.

Jackson, S. E., 2008a, Calibration strategies for elemental analysis by LA-ICP-MS, *in* Sylvester, P., ed., Laser Ablation ICP-MS in the Earth Sciences: Current Practices and Outstanding Issues, Short Course Series Volume 40, Mineralogical Association of Canada, p. 169-188.

Jackson, S. E., 2008b, LAMTRACE data reduction software for LA-ICP-MS, *in* Sylvester, P., ed., Laser Ablation ICP-MS in the Earth Sciences: Current Practices and Outstanding Issues, Short Course Series Volume 40, Mineralogical Association of Canada, p. 305-307.

Jochum, K. P., Nohl, U., Herwig, K., Lammel, E., Stoll, B., and Hofmann, A. W., 2005, GeoReM: a new geochemical database for reference materials and isotopic standards: Geostandards and Geoanalytical Research, v. 29, p. 333-338.

Kobylinski, C., Hatori, K., Smith, S., and Plouffe, A., 2016. Report on the composition and assemblage of minerals associated with the porphyry Cu-Mo mineralization at the Gibraltar deposit, south central British Columbia, Canada; Geological Survey of Canada, Open File 8025, 30 p.

Lawley, C. J. M., Creaser, R. A., Jackson, S. E., Yang, Z., Davis, B. J., Pehrsson, S. J., Dubé, B., Mercier-Langevin, P., and Vaillancourt, D., 2015, Unraveling the Western Churchill Province Paleoproterozoic gold metallotect: constraints from Re-Os arsenopyrite and U-Pb xenotime geochronology and LA-ICP-MS arsenopyrite trace element chemistry at the BIF-hosted Meliadine Gold District, Nunavut, Canada*: Economic Geology, v. 110, p. 1425-1454.

Lawley, C. J. M., Petts, D. C., Jackson, S. E., Zagorevski, A., Pearson, D. G., Kjarsgaard, B. A., Savard, D., and Tschirhart, V., 2020, Precious metal mobility during serpentinization and breakdown of base metal sulphide: Lithos, v. 354-355, p. 105278.

Lee, R. G., Byrne, K., and Lesage, G., 2020, Distal alteration facies of Late Triassic to Early Jurassic porphyry copper deposits, British Columbia, Canada: A green rock perspective, *in* Sharman, E. R., Lang, J. R., and Chapman, J., eds., Porphyry deposits of the Nortwestern Cordillera of North America: A 25-year update, Special volume 57, Canadian Institute of Mining, Metallurgy and Petroleum, p. 68-87.

Orovan, E., and Hollings, P., 2020, Exploring the Green Rock Environment: An Introduction: Economic Geology, v. 115, p. 695-700.

Panteleyev, A., Bailey, D. G., Bloodgood, M. A., and Hancock, K. D., 1996, Geology and mineral deposits of the Quesnel River-Horsefly map area, central Quesnel Trough, British Columbia, British Columbia Ministry of Employment and Investment, 156 p.

Paradis, S., Jackson, S. E., Petts, D., Simandl, G. J., D'Souza, R. J., and Hamilton, T. S., 2022, Distribution of trace elements in pyrite from carbonate-hosted sulfide deposits of southern British Columbia, *in* Peter, J. M., and Gadd, M. G., eds., Targeted Geoscience Initiative 5: volcanic- and sediment-hosted massive-sulfide deposit genesis and exploration methods, Bulletin 617, Geological Survey of Canada, p. 129-163.

Plouffe, A., and Ferbey, T., 2016, Till geochemistry, mineralogy and textural data near four Cu porphyry deposits in British Columbia, 1 .zip file p.

Plouffe, A., and Ferbey, T., 2017, Porphyry Cu indicator minerals in till: A method to discover buried mineralization, *in* Ferbey, T., Plouffe, A., and Hickin, A., eds., Indicator Minerals in Till and Stream Sediments of the Canadian Cordillera, Mineral Association of Canada, Topics in Mineral Sciences Volume 47,

Geological Association of Canada, Special Paper 50, p. 129-159.

Plouffe, A., Ferbey, T., Hashmi, S., and Ward, B. C., 2016, Till geochemistry and mineralogy: vectoring towards Cu porphyry deposits in British Columbia, Canada: Geochemistry: Exploration, Environment, Analysis, v. 16, p. 213-232.

Plouffe, A., Acosta-Góngora, P., Kjarsgaard, I. M., Petts, D., Ferbey, T., and Venance, K. E., 2021a, Detrital epidote chemistry: detecting the alteration footprint of porphyry copper mineralization in the Quesnel terrane of the Canadian Cordillera, British Columbia, *in* Plouffe, A., and Schetselaar, E., eds., Targeted Geoscience Initiative 5: contributions to the understanding and exploration of porphyry deposits, Bulletin 616, Geological Survey of Canada, p. 137-157.

Plouffe, A., Wilton, D. H. C., McNeil, R., and Ferbey, T., 2021b, Automated indicator-mineral analysis of the fine-sand, heavy-mineral concentrate fraction of till: a promising exploration tool for porphyry copper mineralization *in* Plouffe, A., and Schetselaar, E., eds., Targeted Geoscience Initiative 5: contributions to the understanding and exploration of porphyry deposits, Bulletin 616, Geological Survey of Canada, p. 203-223.

Plouffe, A., Kjarsgaard, I. M., Ferbey, T., Wilton, D. H. C., Petts, D. C., Percival, J. B., Kobylinski, C. H., and McNeil, R., 2022, Detecting buried porphyry Cu mineralization in a glaciated landscape: a case study from the Gibraltar Cu-Mo deposit, British Columbia, Canada: Economic Geology, v. 117, p. 777-799.

Rees, C., Gillstrom, G., and Riedell, K. B., 2020, The Mount Polley porphyry copper deposit, south-central British Columbia, *in* Sharman, E. R., Lang, J. R., and Chapman, J., eds., Porphyry deposits of the Nortwestern Cordillera of North America: A 25-year update, Special volume 57, Canadian Institute of Mining, Metallurgy and Petroleum, p. 567-600.

Sillitoe, R. H., 2010, Porphyry Copper Systems: Economic Geology, v. 105, p. 3-41.

Sinclair, W. D., 2007, Porphyry deposits, *in* Goodfellow, W. D., ed., Mineral Deposits of Canada: A synthesis of Major Deposit-Types, District Metallogeny, the Evolution of Geological Provinces, and Exploration Methods, Special Publication No. 5, Geological Association of Canada, Mineral Deposit Division, p. 223-243.

van Straaten, B. I., Mostaghimi, N., Kennedy, L. A., Gallagher, C., Schiarizza, P., and Smith, S., 2020, The deformed Gibraltar porphyry copper-molybdenum deposit, south-central British Columbia, Canada, *in* Sharman, E. R., Lang, J., and Chapman, J., eds., Porphyry Deposits of the Northwestern Cordillera of North America: A 25-Year Update, Special Volume 57, Canadian Institute of Mining, Metallurgy and Petroleum, p. 546-566.

Wilkinson, J. J., Baker, M. J., Cooke, D. R., and Wilkinson, C. C., 2020, Exploration targeting in porphyry Cu systems using propylitic mineral chemistry: a case study of the El Teniente deposit, Chile: Economic Geology, v. 115, p. 771-791.